Sterility and absence of histopathological defects in nonreproductive organs of a mouse ERβ-null mutant

Maria Cristina Antal, Andrée Krust, Pierre Chambon*, and Manuel Mark

Institut de Génétique et de Biologie Moléculaire et Cellulaire, Centre National de la Recherche Scientifique, Institut National de la Santé et de la Recherche Médicale, Collège de France, Université Louis Pasteur de Strasbourg, 67404 Illkirch Cedex, France

Contributed by Pierre Chambon, December 21, 2007 (sent for review October 7, 2007)

Estrogen signaling is mediated by estrogen receptors α (ERα) and β (ERβ). Although a consensus has now been reached concerning many physiological functions of ERα, those of ERβ are still controversial: When housed and examined in two distant laboratories, mice originating from the same initial ERβ mutant exhibited widely different phenotypes, which were themselves different from the phenotype of another ERβ mutant previously generated in our laboratory. Because, in addition to a knockout insertion in exon 3, all these mouse mutants displayed alternative splicing transcripts, we have now constructed a ERβ mouse mutant ($ER\beta_{ST}^{L-/L-}$) in which exon 3 was cleanly deleted by Cre/LoxP-mediated excision and was devoid of any transcript downstream of exon 3. Both females and males were sterile. The histology of the ovary was mildly affected, and no histological defects were detected in other organs, neither in females nor in males. Our present results, which are in contrast with previously published data, suggest that, with the notable exception of male and female reproduction, ERβ is not required in the mouse for the development and homeostasis of the major body systems.

aging | ERβ function | ERβ knockout | estrogen signaling | histopathology

Estrogens have well acknowledged functions in ovary, testis, and male and female reproductive tracts (1–4) that are mediated through the nuclear receptors isotypes estrogen receptors α (ERα) (5, 6) and β (ERβ) (7–9). In addition, numerous clinical and animal model studies have pointed to estrogen functions in bone, adipose tissue, brain, and immune and cardiovascular systems and have suggested the potential usefulness of estrogen receptor modulators in the prevention and/or clinical management of osteoporosis, obesity, breast cancers, and neurodegenerative and autoimmune diseases (2–4, 10, 11).

Although a consensus has been reached concerning many physiological functions of ERα, those of ERβ are still controversial (12). To date, several genetically engineered mice aimed at functionally ablating the ERβ gene have been generated and analyzed in different laboratories. Krege *et al.* (13) disrupted the mouse ERβ gene ($ER\beta KO_{CH}$) (see ref. 12 for ERβ mutant nomenclature) by inserting a *neo* cassette in the 3′ to 5′ orientation into PstI site of exon 3, which encodes the first zinc finger of the DNA-binding domain (DBD). The full-length ERβ mRNA was not detected in the mutant mouse, which, nevertheless, expressed several transcript variants where exon 3 was consistently spliced out. The $ER\beta KO_{CH}$ mouse colony was subsequently duplicated and transferred to Karolinska Institute ($ER\beta KO_{KI}$). Dupont *et al.* (14) generated an independent ERβ mutant mouse line by inserting the *neo* cassette in the 5′ to 3′ orientation into the SpI site of the exon 3 ($ER\beta KO_{ST}$). As in the case of $ER\beta KO_{CH}$, several splice variants lacking exon 3 were detected in this mutant. Moreover, Shughrue *et al.* (15) reported the disruption of the ERβ gene by insertion of stop codons in all three reading frames and of a *neo* cassette in intron 1. This strategy resulted in the truncation of exons 1 and 2 encoding the A/B domain and the N-terminal half of the DBD and in a deletion of intron 1 ($ER\beta KO_{WY}$).

Morphological analysis of $ER\beta KO_{CH}$ mutant line revealed a hyperplasia of prostatic epithelium (13), whereas examination of $ER\beta KO_{KI}$ mutant line (16) indicated the presence of prostatic intraepithelial hyperplasia (PIN). In addition, examination of the $ER\beta KO_{KI}$ line supported an involvement of ERβ in the development and/or maintenance of several neuronal populations of the brain (17, 18). However, lesions reported in the ventral prostate of $ER\beta KO_{CH}$ and $ER\beta KO_{KI}$ males were not found in the $ER\beta KO_{ST}$ line (14). Because a low frequency of prostate lesions in old $ER\beta KO_{ST}$ males might have been overlooked due to the small number of samples analyzed (14), we subsequently examined a larger group ($n > 15$) of 20-month-old $ER\beta KO_{ST}$ males for possible prostate lesions (our unpublished results). In the same study, we also characterized the status of the brain in $ER\beta KO_{ST}$ males. Unexpectedly, we found that prostates and brains of $ER\beta KO_{ST}$ mice, in contrast to their counterparts in $ER\beta KO_{KI}$ mice, were indistinguishable from those of our WT littermates (our unpublished results).

In all of the above disruptions of the ERβ gene several transcript variants were found, encoding putative truncated peptides lacking the DBD and ligand binding domain (13–15) or the DBD only (13). To eliminate any possible phenotypic effect of these transcript variants, we decided to generate an ERβ-null mutant, hereafter referred to as $ER\beta_{ST}^{L-/L-}$, in which exon 3 was deleted through Cre/LoxP-mediated excision and which was devoid of any transcript downstream of exon 3. We report here the characterization of these $ER\beta_{ST}^{L-/L-}$ mutants, which do not display morphological defects in the prostate, in contrast to $ER\beta KO_{CH}$ and $ER\beta KO_{KI}$ mutants (13, 16, 19), or, in contrast to $ER\beta KO_{KI}$ mutants, defects in the brain (17), lymphoid tissues (20), heart (21), lung (22, 23), colon (24), and urinary bladder (25).

Results and Discussion

Generation of a ERβ-Null Mouse ($ER\beta_{ST}^{L-/L-}$), Characterization of Its Reproductive Function, and General Pathophysiological Analysis. To generate a fully disrupted ERβ mutant, we used the Cre/loxP strategy. Chimeric males derived from mutant ES clones transmitted the mutation through their germ line. We identified mice in which all of the sequences located between the loxP sites flanking ERβ exon 3 were excised (L-allele) [supporting information (SI) Fig. 5*a* and *SI Materials and Methods*].

The inactivation of the ERβ gene was first indicated by the absence of ERβ protein in prostate and testis of homozygous $ER\beta^{L-/L-}$ mice (SI Fig. 5*b* and *SI Materials and Methods*). The characterization of the ERβ transcripts by RT-PCR, using total RNAs extracted from uterus (SI Fig. 5*c*) and ovaries (data not

Author contributions: A.K. and M.M. designed research; M.C.A., A.K., and M.M. performed research; M.C.A., A.K., P.C., and M.M. analyzed data; and M.C.A., A.K., P.C., and M.M. wrote the paper.

The authors declare no conflict of interest.

*To whom correspondence should be addressed. E-mail: chambon@titus.u-strasbg.fr.

This article contains supporting information online at www.pnas.org/cgi/content/full/0712029105/DC1.

shown) of WT, ERβ$^{+/L-}$ and ERβ$^{L-/L-}$ mice unambiguously confirmed that the ERβ mutation was a null mutation, because all of the expected reverse transcription products of ERβ mRNA were obtained with WT (+/+) and ERβ$^{+/L-}$ RNAs, whereas no transcript downstream exon 3 could be detected in ERβ$^{L-/L-}$ mice, hereafter called ERβ$_{ST}^{L-/L-}$ mutants (SI Fig. 5*c*, *SI Materials and Methods*, and data not shown).

Five-month-old (hereafter referred to as "young") and 16- to 19-month-old (hereafter referred to as "old") ERβ$^{L-/L-}$ mutants and their wild-type (WT) male and female littermates were subjected to systematic biochemical, hematological, macroscopical, and histopathological analyses. Biochemical and hematological parameters were determined in old mice.

Young and old ERβ$^{L-/L-}$ and WT mice displayed no statistically significant differences with respect to body and organ weights (SI Fig. 6) and, with the exception of ovaries, ERβ$_{ST}^{L-/L-}$ organs appeared normal on histological sections stained with hematoxylin and eosin (SI Table 1, below, and data not shown). An extensive clinical chemistry and hematological examination did not reveal relevant differences between the ERβ$_{ST}^{L-/L-}$ and WT mice (SI Fig. 7). Additional investigations were nevertheless performed on organs, which, in ERβKO$_{KI}$ mice, displayed histological defects, either already in young adults, i.e., mammary glands, colon, and urinary bladder, or at advanced ages, i.e., brain, prostate, bone marrow, spleen, heart, and lung (for references, see Introduction).

Sterility and Reproductive System in ERβ$_{ST}^{L-/L-}$ Mutant Mice. ERβ$_{ST}^{L-/L-}$ females/males were continuously mated with fertile males/females. Because no vaginal plugs were observed in fertile females after mating with ERβ$_{ST}^{L-/L-}$ males and as no pregnancy was produced in ERβ$_{ST}^{L-/L-}$ females by fertile males, we concluded that both females and males mutants are sterile. Testis and epididymis histology of ERβ$^{L-/L-}$ males were normal, and their spermatozoa appeared normally mobile (data not shown).

To determine whether an ovulation defect could cause the infertility in female mutants, we performed superovulation experiments, using ERβ$_{ST}^{L-/L-}$ and WT females. No oocytes were found in any of the mutant females tested (n = 19), compared with a mean number of 46 oocytes per WT female (n = 8). Histological examination of ovaries from 5-month-old ERβ$_{ST}^{L-/L-}$ females revealed the presence of (*i*) follicles at various stages of development, ranging from primordial to large antral; (*ii*) rare (i.e., mean of 0.5 corpora lutea per ovary in ERβ$_{ST}^{L-/L-}$ mutants versus 2.5 corpora lutea per ovary in WT mice; n = 5), but morphologically normal corpora lutea (SI Fig. 8 *a* and *b*); (*iii*) morphologically normal thecal cell layer (SI Fig. 8 *c–f*); (*iv*) a higher amount of stromal collagen compared with age-matched WT mice (SI Fig. 8 *g* and *h*); and (*v*) an increased number of atretic follicles (i.e., mean of 2.4 atretic follicles per ovary in ERβ$_{ST}^{L-/L-}$ mutants versus 1.25 atretic follicles per ovary in WT mice; n = 5) (data not shown). Uterus histology of ERβ$_{ST}^{L-/L-}$ females was normal (data not shown). The reduced number of corpora lutea is in accordance with data obtained on ERβKO$_{CH}$ (13) and ERβKO$_{ST}$ mutants (14), and an increased follicle atresia was also detected in ERβKO$_{CH}$ mutants (13). However, ERβ$_{ST}^{L-/L-}$ mutants do not display the increased collagen deposits and decreased vascularization of the theca layer reported in ERβKO$_{KI}$ ovaries (26).

The ovarian cycle of virgin 8-month-old ERβ$_{ST}^{L-/L-}$ mice and of their WT littermates (n = 4 for each genotype) was assessed daily from the vaginal smear aspect and staged according to (27) in proestrus, estrus, metestrus I, metestrus II, and diestrus stages (SI Fig. 9 and data not shown) over a 24-day period. In two of the 8-month-old ERβ$_{ST}^{L-/L-}$ mice the ovarian cycle was irregular, varying between 6 and 10 days, and no proestrus, estrus, and metestrus I stages were ever detected (SI Fig. 9 *d–f*). These three stages were replaced by a single abnormal stage in which the vaginal smear contained mainly nonnucleated epithelial cells intermingled with nucleated epithelial cells and polymorphonuclear neutrophils (SI Fig. 9*d*). The two other ERβ$_{ST}^{L-/L-}$ mice had no ovarian cycling activity and displayed only the abnormal vaginal smear (SI Fig. 9*d*). Thus, even though the histology of ERβ$_{ST}^{L-/L-}$ ovaries appears mildly affected, their function is impaired.

The morphology of mammary glands from 5- and 8-month-old ERβ$_{ST}^{L-/L-}$ (SI Fig. 10 *d* and *e*) females was examined. At both ages the aspect of the ERβ$_{ST}^{L-/L-}$ mammary gland was identical with that of a metestrus WT mammary gland, which exhibit a ductal system without terminal end buds and alveolar buds (SI Fig. 10 *a*, *b*, *d*, and *e* and ref. 28). It seems that, in the absence of a normal ovarian cycle (see above), ERβ$_{ST}^{L-/L-}$ females can establish the normal ductal system seen in WT metestrus but fail to generate the progesterone-induced side branching seen in WT diestrus (SI Fig. 10*c* and ref. 28). We also looked for possible age-related pathological modifications (29) and found that mammary glands from 19-month-old ERβ$_{ST}^{L-/L-}$ females were indistinguishable from those of age-matched WT littermates and, in particular, that there was no cystic dilatation of ductal structures (SI Fig. 10 *f–i*).

In contrast to our results, Couse and Korach (1) have reported that ductal structure of glands from virgin ERβKO$_{CH}$ females and differentiation of lactating glands are both normal, whereas Förster *et al.* (30) reported normal ductal development but impaired side branching and alveolar development in glands from virgin and lactating ERβKO$_{KI}$ females, respectively. Furthermore, Palmieri *et al.* (29) described an age-related "severe cystic breast disease," which is in contrast to our data showing normal histological aspect of the mammary glands in old ERβ$_{ST}^{L-/L-}$ females.

Normal Morphology, Cell Proliferation, and Apoptosis in ERβ$_{ST}^{L-/L-}$ Prostates. The mouse prostate is composed of three paired lobes: anterior prostate, ventral prostate, and dorsolateral prostate lobes (31). Ventral prostate lobes of 5- and 16-month-old ERβ$_{ST}^{L-/L-}$ and WT males contained two types of secretory units (called prostate alveoli): (*i*) alveoli lined by a low-cuboidal to flattened epithelium displaying few folds (Fig. 1 *a* and *b*) and (*ii*) "functionally hyperplastic" alveoli lined by a columnar and extensively folded epithelium (Fig. 1 *a–d* and ref. 31). Examination of three sections containing ventral, dorsal, and anterior prostate samples from 5-month-old ERβ$_{ST}^{L-/L-}$ (n = 3) prostate did not reveal histological anomalies. Serially sectioned prostates from four 16-month-old ERβ$_{ST}^{L-/L-}$ and four age-matched WT mice were then examined. In these mice, various atypical (i.e., karyomegaly and hyperchromatic) nuclei were present either in quiescent alveoli or in functionally hyperplastic alveoli with the same low frequency in ERβ$_{ST}^{L-/L-}$ and WT ventral (SI Fig. 11 *a–f* and *h*) and dorsolateral prostate lobes (SI Fig. 11*g*). With respect to cytoplasmic atypia, the incidence of epithelial cells vacuolization was significantly lower in the ventral prostate of ERβ$_{ST}^{L-/L-}$mutants, but the physiological significance of this vacuolization, if any, is unknown. A single case of true epithelial hyperplasia (i.e., a papillary outgrowth of the epithelium; ref. 32) was detected in a WT male out of four (SI Fig. 11 *e*, *f*, and *h*). Thus, the histological aspect of the ventral prostate epithelium of the 16-month-old ERβ$_{ST}^{L-/L-}$ analyzed on serial histological sections was essentially similar to its counterpart in aged-matched WT males. Likewise, histological analysis of 16-month-old ERβ$_{ST}^{L-/L-}$ dorsolateral and anterior prostate lobes failed to reveal differences with their counterparts in WT males. The absence of specific histological lesions in ventral prostate of 16-month-old ERβ$_{ST}^{L-/L-}$ mutants is in sharp contrast with defects reported in the ERβKO$_{KI}$ ventral prostatic epithelium, which displays multiple hyperplastic foci, readily visible at 5

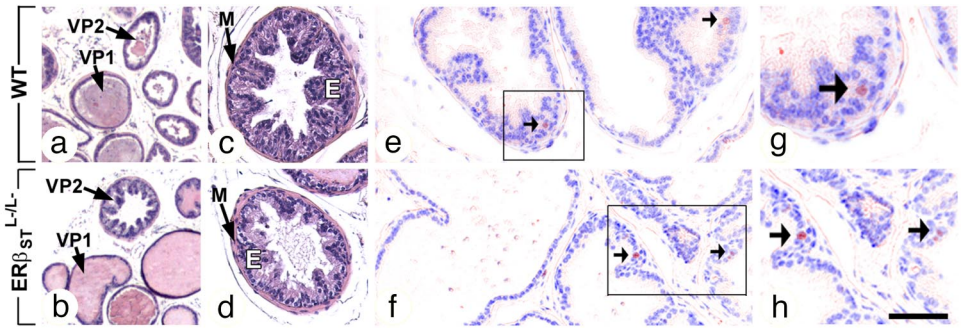

Fig. 1. Normal morphology and cell proliferation in the ventral prostate of 16-month-old ER$\beta_{ST}^{L-/L-}$ mice. (*a–d*) Hematoxylin and eosin-stained sections of ventral prostate. (*c* and *d*) Higher magnification of functionally hyperplastic alveoli. (*e–h*) Immunostaining for detection of the cell proliferation marker Ki67 in ventral prostate. Arrows point to Ki67-positive epithelial cells (red signals). (*g* and *h*) Enlargement of the black frames from *e* and *f*, respectively. E, prostatic epithelium; M, smooth muscle; VP1 and VP2, alveoli without and with functional hyperplasia, respectively. Four males of each genotype were used in each type of assay. (Scale bar: *a* and *b*, 500 μm; *c–f*, 50 μm.)

months, and affecting 80% of mutants by 12 months of age (13, 16, 33).

To further assess epithelial homeostasis in ventral and dorsolateral prostate lobes of 16-month-old ER$\beta_{ST}^{L-/L-}$ mutants, we investigated cell proliferation and apoptosis through immunohistochemical detection of the proliferation marker Ki67 and TUNEL assays, respectively (n = 4). Ki67-positive cells were rare and proliferation indices (i.e., ratios between Ki67-positive nuclei and total number of nuclei stained with DAPI) were not significantly different between ER$\beta_{ST}^{L-/L-}$ and WT prostate epithelia (Fig. 1 *e–h* and SI Fig. 11*i*). These observations are consistent with previous reports showing very low proliferation rates in the WT mouse prostate (14, 34) and in its ERβKO$_{ST}$ counterpart (ref. 14 and data not shown). However, they are in sharp contrast with results from ref. 19, showing that most epithelial cells in ventral prostate lobes of 12-month-old ERβKO$_{KI}$ males stain positively for Ki67. We also explored apoptosis in ventral and dorsal prostates of 16-month-old ER$\beta_{ST}^{L-/L-}$ and WT mice. No apoptotic epithelial cell was detected on the sections analyzed (data not shown). We conclude that there are no differences between 16-month-old ER$\beta_{ST}^{L-/L-}$ and WT males with respect to prostate morphology, proliferation indices and apoptosis of epithelial cells.

The Brain of 16-Month-Old ER$\beta_{ST}^{L-/L-}$ Mutant Males Is Morphologically Normal. The analysis was focused on the somatosensory cortex of 16-month-old ER$\beta_{ST}^{L-/L-}$ mutant males, because severe alterations of this structure were recorded in aging ERβKO$_{KI}$ males (17). In old ER$\beta_{ST}^{L-/L-}$ males (n = 5), the thickness of the somatosensory cortex was normal (Fig. 2 *a* and *b*), and five layers, differing in neuron morphology, were clearly identified, namely the molecular (I), small pyramidal (II + III), granular (IV), large pyramidal (V), and polymorphic (VI) cell layers (Fig. 2 *c* and *d* and data not shown), which were indistinguishable from their counterparts in aged-matched WT males. Somatosensory cortex neurons that were identified as cells displaying a large nucleus containing finely dispersed chromatin and a prominent nucleolus (35) were counted. No difference could be found between ER$\beta_{ST}^{L-/L-}$ and WT males in any of the five layers (SI Fig. 12*b*). In addition, glial fibrillary acidic protein (GFAP) staining of brain sections did not reveal significant differences in the number of glial cells between mutant and WT brain regions, including the paraventricular nucleus of the hypothalamus (compare Fig. 2*e* with Fig. 2*f*), medial amygdala (compare Fig. 2*g* with Fig. 2*h*), and medial preoptic nucleus (data not shown). Moreover, no significant difference in cerebral hemisphere weight was detected between old ER$\beta_{ST}^{L-/L-}$ and WT males and females (n = 7) (SI Fig. 12*a*). Similar results were obtained in ERβKO$_{ST}$ mutants (data not shown).

Wang *et al.* (17) described the ERβKO$_{KI}$ somatosensory cortex: "the overall structure is disorganized with no clear evidence of layers II, III, IV and V". In addition, the ERβKO$_{KI}$ brain exhibits neuronal hypocellularity in the same cortical layers, and astrogliosis in the medial preoptic area, paraventricular nucleus of hypothalamus and medial amygdala nucleus

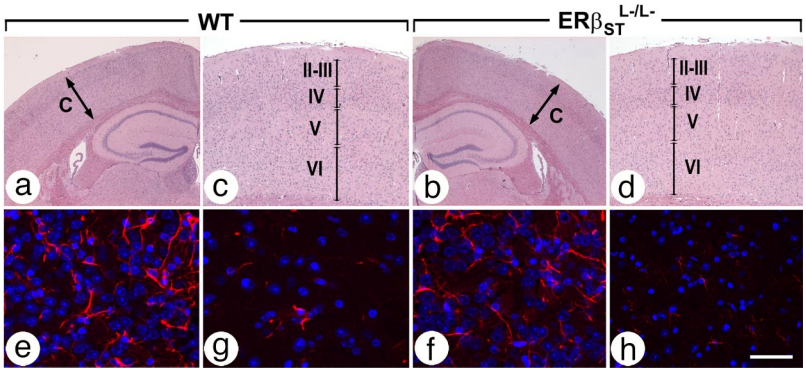

Fig. 2. The ER$\beta_{ST}^{L-/L-}$ mutation does not alter architecture and neuronal density of the somatosensory cortex and does not elicit astrocytosis in 16-month-old mice. (*a–d*) Coronal sections at similar levels of the brains of WT and ER$\beta_{ST}^{L-/L-}$ males. (*e–h*) Immunodetection of GFAP (red signals) and DAPI counterstain (blue nuclei) in the paraventricular nucleus (*e* and *f*) and amygdala (*g* and *h*). C, cerebral cortex. Five males of each genotype were used for histology. (Scale bar: *a* and *b*, 500 μm; *c* and *d*, 250 μm; *e–h*, 30 μm.)

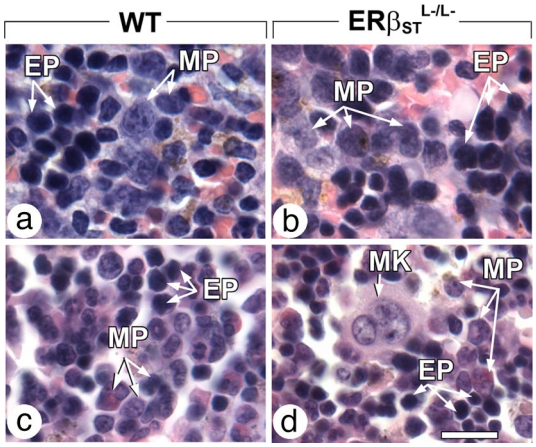

Fig. 3. Absence of myeloproliferation in 16- to 19-month-old ER$\beta_{ST}^{L-/L-}$ mice. (*a–d*) Sections of hematopoietic compartment of the spleen (*a* and *b*) and bone marrow (*c* and *d*) of ER$\beta_{ST}^{L-/L-}$ females (hematoxylin and eosin). Myeloid precursors (MP) appear as large cells, containing (*i*) a large, pale-stained nucleus displaying prominent nucleoli and a finely granular chromatin and (*ii*) a relatively low abundance of lightly stained cytoplasm. In contrast, erythroid precursors (EP) are medium- to small-sized cells, with dark nuclei and low amount of darkly stained cytoplasm. MK, megakaryocyte. Nine mice of each sex and genotype were used for histology. (Scale bar: 8 μm.)

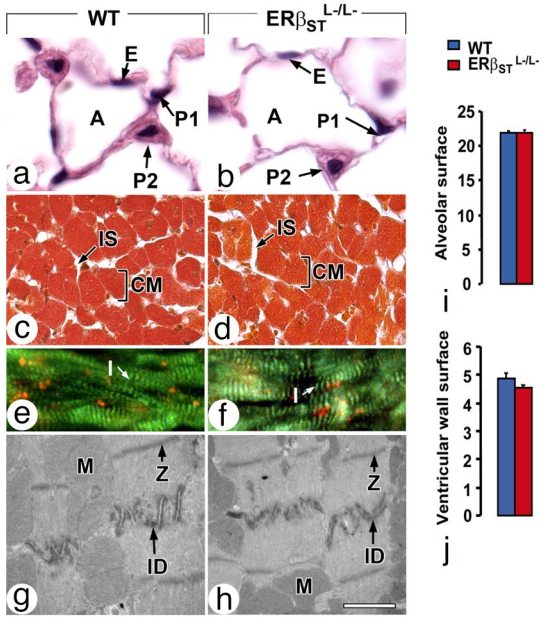

Fig. 4. Normal morphology of the lung and heart of 16- to 19-month-old ER$\beta_{ST}^{L-/L-}$ mice. (*a* and *b*) Normal cellular composition of the lung of ER$\beta_{ST}^{L-/L-}$ females (hematoxylin and eosin). (*c* and *d*) Normal cardiomyocyte size and intercellular spaces in the heart of ER$\beta_{ST}^{L-/L-}$ males (modified Mallory's trichrome). (*e* and *f*) Normal pattern of f-actin distribution in the sarcomeres of ER$\beta_{ST}^{L-/L-}$hearts; sections are stained with FITC-conjugated phalloidin. (*g* and *h*) Normal structure of intercalated discs in ER$\beta_{ST}^{L-/L-}$ hearts; transmission electron microscopy. (*i*) Normal mean alveolar surface in ER$\beta_{ST}^{L-/L-}$ female lungs (arbitrary units; pixels $\times$ 10^3; means $\pm$ SEM). (*j*) Normal mean left ventricular wall surface in ER$\beta_{ST}^{L-/L-}$ male heart (arbitrary units; pixel $\times$ 10^5; means $\pm$ SEM). A, alveolar lumen; CM, cardiomyocytes; E, endothelial cell; I and Z, I and Z bands, respectively; ID, intercalated disk; IS, intercellular spaces; M, mitochondria; P1 and P2, type 1 and 2 pneumocytes, respectively. Nineteen-month-old females of each genotype were used, 10 for histological analysis and 5 for alveolar surface measurement; 16-month-old males of each genotype were used, 8 for evaluation of cardiomyocytes size and left ventricle wall surface, 5 for f-actin staining and 3 for electron microscopy. (Scale bar: *a* and *b*, 40 μm; *c–f*, 100 μm; *g* and *h*, 2 μm.)

in 2-month-old mutants (17); moreover, by 2 years of age, the ERβKO$_{KI}$ brain appeared grossly atrophic (17). Clearly, the disorganization of cortical architecture, hypocellularity of cerebral cortex, astrocytosis, and brain atrophy that have been reported to be hallmarks of the ERβKO$_{KI}$ mutant phenotype are all lacking in our present ER$\beta_{ST}^{L-/L-}$ mutants and in our previous ERβKO$_{ST}$ mutants (ref. 14 and data not shown).

Lymphoid Organs of 16- to 19-Month-Old ER$\beta_{ST}^{L-/L-}$ Mutants Appear Normal. Mean spleen weights were not significantly different in old ER$\beta_{ST}^{L-/L-}$ mutant and in WT males and females (SI Fig. 6). Histological analysis of these ER$\beta_{ST}^{L-/L-}$ mutants did not reveal any evidence of myeloproliferation in spleen (Fig. 3 *a* and *b*) and bone marrow (Fig. 3 *c* and *d*), and of myeloid infiltrates in nonhematopoietic organs (n = 9) (e.g., lungs, livers, and kidneys; data not shown). Peripheral blood in ER$\beta_{ST}^{L-/L-}$ mice (n = 10 for males and n = 7 for females) was normal with respect to the total number of white blood cells, and lymphocyte, granulocyte, and monocyte numbers (SI Fig. 7 and SI Fig. 12 *c–e*). Likewise, FACS analysis of spleen and bone marrow from 19-month-old ER$\beta_{ST}^{L-/L-}$ females (n = 4) were normal with respect to total cells count and to myelocyte and B-lymphocyte numbers (SI Fig. 12 *f* and *g*).

In contrast, ERβKO$_{KI}$ mice were reported to develop by one year of age a marked splenomegaly accompanied by (*i*) granulocyte infiltration of liver and lung, (*ii*) an increased number of leukocytes in peripheral blood, and (*iii*) an increased number of granulocytes in bone marrow (20). We conclude that, in striking contrast to ERβKO$_{KI}$ mutants, ER$\beta_{ST}^{L-/L-}$ mutants do not display hematological abnormalities.

Normal Heart and Lung Morphology in ER$\beta_{ST}^{L-/L-}$ Mutants. Lung alveoli of ER$\beta_{ST}^{L-/L-}$ females were carefully examined, because various alterations of these structures were recorded in ERβKO$_{KI}$ females (22, 23). We first compared alveoli of 19-month-old ER$\beta_{ST}^{L-/L-}$ and WT females (n = 10) on histological sections stained with hematoxylin and eosin. No difference in thickness and cellular composition of alveolar walls (comprising endothelial cells and type 1 and 2 pneumocytes) and in the content of alveolar lumens was observed (Fig. 4 *a* and *b*). Additionally, upon staining with sirius red, fibrillar collagen deposits were undetectable in alveoli of these old ER$\beta_{ST}^{L-/L-}$ females (n = 4) (SI Fig. 13 *a* and *b*), and morphometric assessment of alveolar surface between ER$\beta_{ST}^{L-/L-}$ and WT females yielded no significant difference (n = 5) (Fig. 4*i*). Therefore, the lungs defects reported in ERβKO$_{KI}$ females (22, 23), namely (*i*) larger and fewer alveoli than in WT females; (*ii*) large areas of unexpanded alveoli; (*iii*) increased collagen deposits in alveolar walls; and (*iv*) by the age of 1 year, surfactant accumulation in alveolar spaces were all absent in ER$\beta_{ST}^{L-/L-}$ females.

Heart morphology was investigated in 16-month-old males. No significant differences in heart weight (SI Fig. 6), cardiomyocyte size and intercellular space (Fig. 4 *c* and *d*), and left ventricle wall surface (Fig. 4*j*) were observed between ER$\beta_{ST}^{L-/L-}$ mutants and their WT littermates (n = 8). It appears, therefore, that 16-month-old ER$\beta_{ST}^{L-/L-}$ males do not exhibit signs of cardiac hypertrophy, in contrast to ERβKO$_{KI}$ males that show enlarged hearts, cardiomyocytes, and intercellular spaces by 8 months of age (21). Phalloidin staining of sarcomere I-bands (Fig. 4 *e* and *f*) did not show differences in myofibrils parallelism, and ultrastructural analysis of the left ventricular myocardium did not reveal abnormalities in size and morphology of intercalated discs (Fig. 4 *g* and *h*). These observations are in marked contrast with those made with ERβKO$_{KI}$ male hearts, which display irregular orientation of their myofibrils and disrupted intercalated discs

(21). The heart of females, which was also reported to exhibit features of hypertrophy in the ERβKO$_{KI}$ mutants (21), was not investigated in our ERβ$_{ST}^{L-/L-}$ mutants.

The ERβ$_{ST}^{L-/L-}$ Urinary Bladder and Colon Display a Normal Structure. The bladder, proximal, and distal colon of 5-month-old male ($n = 6$) and female ($n = 6$) ERβ$_{ST}^{L-/L-}$ mutants were analyzed on histological sections stained with hematoxylin and eosin. In addition, alcian blue staining was used to visualize acid mucins in intestinal goblet cells (36). No difference was observed with respect to bladder histology (SI Fig. 14 *g* and *h*), colon cells populations (SI Fig. 14 *a–d*), and acid mucins distribution (SI Fig. 14 *e* and *f*) between ERβ$_{ST}^{L-/L-}$ mutants and age-matched WT mice. In contrast, the bladder of females and colon of both sexes of young ERβKO$_{KI}$ have been reported to display defects that correct with aging (24, 25). More specifically, in young female ERβKO$_{KI}$ mice, the bladder was reported to develop features resembling human interstitial cystitis in females (25) and, in both sexes, the colon exhibited severe subepithelial lymphoid infiltrates predominantly in its proximal portion and an abnormal mucin distribution in its distal portion (24). We conclude that the bladder and colon of our ERβ$_{ST}^{L-/L-}$ mutants lack the morphological abnormalities that were found in young ERβKO$_{KI}$ mutants.

Conclusions

The discovery of ERβ (7–9) has rejuvenated the field of estrogen receptor research (reviewed in refs. 2, 11, and 12). To investigate the physiological functions of this receptor, four groups have independently characterized mutant mouse lines bearing loss-of-function mutations of the ERβ gene, namely the ERβKO$_{CH}$ (13), ERβKO$_{KI}$ (reviewed in ref. 11), ERβKO$_{ST}$ (14), and ERβKO$_{WY}$ (15) lines. Even though a perfect match between the phenotypes of ERβ mutant mouse lines was not to be expected, the phenotypic differences between ERβKO$_{CH}$, ERβKO$_{KI}$, and ERβKO$_{ST}$ are puzzling (12), particularly in the case of ERβKO$_{CH}$ and ERβKO$_{KI}$, which originate from the same mutant colony. With the hope to uncover, at least partially, the origin of these differences, we generated a fifth mutant mouse line, ERβ$_{ST}^{L-/L-}$, by Cre/LoxP-mediated deletion of exon 3 that encodes the first zinc finger of the ERβ DBD. In contrast to the previously generated ERβ mutants, no ERβ transcript of any exons located downstream of exon 3 and no epitope reacting with an antibody directed against the F region of ERβ could be detected in these ERβ$_{ST}^{L-/L-}$ mutants (see Introduction). Thus, we conclude that the ERβ$_{ST}^{L-/L-}$ mouse is a genuine null mutant.

We undertook a series of pathophysiological investigations on ERβ$_{ST}^{L-/L-}$ mice that encompass clinical biochemistry, FACS analyses, necropsy and histology of a number of organs and systems, morphometry, and electron microscopy. We conclude that ERβ$_{ST}^{L-/L-}$ mice of both sexes are sterile, in contrast to previous reports mentioning hypofertility in females and normal fertility in males in ERβKO$_{CH}$ (13) and ERβKO$_{ST}$ lines (14). The origin for the sterility of ERβ$_{ST}^{L-/L-}$ males is unknown, because their gonads and internal genital organs are histologically normal and the mobility of their spermatozoa appears also normal. It is, however, possible that the epididymis, vas deferens, seminal vesicle, and/or prostate gland, which all express ERβ in WT mice (ref. 37 and references therein) may not be fully functional in ERβ$_{ST}^{L-/L-}$ males, leading to impairment of sperm function(s) that is (are) critical for fertilization. Alternatively, the absence of ERβ may negatively interfere with male sexual behavior, because, in WT mice, ERβ is expressed in neurons from the medial preoptic area and amygdala (ref. 38 and references therein), which are known to play important roles in male sexual behavior. Along the same lines, it is interesting that ERβKO$_{CH}$ mice display a delay with respect to the age at which the first ejaculation occurs (39), although their sexual behavior appears to be otherwise normal (40, 41). In addition, recent data implicate ERβ in the processes of defeminization of the male brain (42) and potentiation of male aggressive behavior (40).

The ERβ$_{ST}^{L-/L-}$ female sterility is due to their incapacity to ovulate. The lack of ovulation, resulting in an absence of estrus cycles, impairs mammary gland development. ERβ$_{ST}^{L-/L-}$ mammary glands correspond to a WT mammary gland blocked at metestrus, in which the ductal system is normally formed, and the alveolar buds are lacking. This is in contrast with mammary glands of ERβKO$_{CH}$ (1, 13) and ERβKO$_{KI}$ (29, 30) mice, which are hypofertile, undergo pregnancy and lactation, and develop alveolar buds.

Our ERβ$_{ST}^{L-/L-}$ mutant mice do not display abnormalities of the (*i*) ventral prostate morphology, epithelial proliferation, and apoptosis; (*ii*) brain morphology and cerebral cortex layers organization, thickness, and cellularity; (*iii*) heart morphology, morphometry, and ultrastructure; (*iv*) lung alveolar size and content; (*v*) goblet cells disposition and mucinous content in the colon; (*vi*) total and population-specific cellularity of hematopoietic organs; and (*vii*) urinary bladder histology. In all of these organs and systems, our present observations are in sharp contrast with the extensive alterations reported in ERβKO$_{KI}$ mice prostate (13, 16, 19), brain (17), hematopoietic organs (20), heart (21), lung (22, 23), colon (24), and bladder (25) (see *Results* and SI Fig. 5–14). However, the normality of the prostate and brain of ERβ$_{ST}^{L-/L-}$ mice is in accordance with our previous results in ERβKO$_{ST}$ mice (ref. 14 and Introduction). Interestingly, the absence of defects in aging prostates has also been mentioned in the case of ERβKO$_{CH}$ mice in review articles (43), but whether the ERβKO$_{CH}$ mutation affects the structure of nonreproductive organs is unknown. To our knowledge, no morphological data concerning ERβKO$_{WY}$ (15) mice are available.

In conclusion, differences in environmental and genetic backgrounds and the presence of different transcript variant, which are particular to each mutant, may possibly account for the relatively minor phenotypic differences displayed by the ERβKO$_{CH}$, ERβKO$_{ST}$, and ERβ$_{ST}^{L-/L-}$ mutants (ref. 12 and this article). However, it is more difficult to conceive how such differences could provide a plausible explanation for the highly pleiotropic pathologies displayed by ERβKO$_{KI}$ mutants and the relative scarcity of defects exhibited by our previous (14) and present ERβKO mutants and even more so by the Chapel Hill ERβKO$_{CH}$ mutants. To solve these puzzling discrepancies, mice from Chapel Hill and Strasbourg colonies should be housed at Karolinska Institute, and their phenotype should be assessed at old ages. Reciprocally, young mice from Karolinska Institute colony should be housed in Chapel Hill and Strasbourg husbandries and examined at old ages.

Our present ERβ$_{ST}^{L2/L2}$ conditional mutant line provides a useful tool to further dissect the function of ERβ through cell type-/time-specific Cre-mediated ablation.

Materials and Methods

Morphology, Immunohistochemistry, and Morphometry. For routine histology, organs were dissected, fixed in 4% (wt/vol) buffered formaldehyde, and embedded in paraffin, except testes that were fixed in Bouin's fluid. Slides were analyzed by four independent observers competent in mouse histopathology. Neurons were counted (17). For electron microscopical analyses, myocardium from heart apex was immersion-fixed in 2.5% glutaraldehyde/2.5% paraformaldehyde in 0.1 M sodium cacodylate buffer. Staining of mammary gland in whole-mounts was performed according to the Eumorphia standard operating procedure (http://empress.har.mrc.ac.uk). F-actin was stained by using fluorescent phalloidin. TUNEL assays were performed according to manufacturer instructions (Chemicon International). The proliferation marker Ki67 and the glial fibrillary acidic protein (GFAP) were detected according to standard immunohistochemical procedures (see *SI Materials and Methods* for details).

Twenty photomicrographs at a ×20 magnification (lung) and one image encompassing the circumference of the left ventricle (sectioned transversally according to ref. 21) were acquired for each mouse. The photomicrographs

were converted to black and white bitmap images, using Photoshop. White areas represent surfaces of interest (i.e., total alveolar space or left ventricular wall), which were then measured by using a home-made algorithm. Total alveolar space surface was further divided by the number of alveoli to calculate, in each image, the mean alveolar surface. A CD containing all figures at high resolution is available upon request.

Clinical Chemistry and FACS Analyses. Blood was collected by intracardiac puncture. Clinical chemistry were performed according to Eumorphia recommendations (http://empress.har.mrc.ac.uk). FACS analyses were performed as described in *SI Materials and Methods*.

ACKNOWLEDGMENTS. We thank Dr. L. M. Garcia-Segura (Consejo Superior de Investigaciones Científicas, Madrid, Spain) and Dr. Jacqueline Trouillas (Institut Fédératif de Recherche 62, Lyon, France) for an expert and a critical comparative examination of histological sections of WT and ER$\beta_{ST}^{L-/L-}$ mice and Dr. Cathrin Brisken (Institut Suisse de Recherche Expérimentale sur le Cancer, Lausanne, Switzerland) and Dr. Heather Harris (Wyeth Research, Collegeville, PA) for a critical reading of the manuscript and suggestions. We acknowledge the technical assistance of Jean-Marie Garnier, Lourdes Ponce-Perez, Thomas Ding, Muriel Klopfenstein, and Fabrice Augé. This work was supported by the European project Estrogen in Women Aging Contract LSHM-CT-2005-518245 and the Association pour la Recherche a l'Institut de Génétique et de Biologie Moleculaire et Cellulaire.

1. Couse JF, Korach KS (1999) Estrogen receptor null mice: What have we learned and where will they lead us? *Endocrine Rev* 20:358–417.
2. Mueller SO, Korach KS (2001) Estrogen receptors and endocrine diseases: Lessons from estrogen receptor knockout mice. *Curr Opin Pharmacol* 1:613–619.
3. Korach KS, *et al.* (2003) Update on animal models developed for analyses of estrogen receptor biological activity. *J Steroid Biochem Mol Biol* 86:387–391.
4. Hewitt SC, Harrell JC, Korach KS (2005) Lessons in estrogen biology from knockout and transgenic animals. *Annu Rev Physiol* 67:285–308.
5. Walter P, *et al.* (1985) Cloning of the human estrogen receptor cDNA. *Proc Natl Acad Sci USA* 82:7889–7893.
6. Green S, *et al.* (1986) Human estrogen receptor cDNA: Sequence, expression and homology to *v-erb-A*. *Nature* 320:134–139.
7. Kuiper GG, Enmark E, Pelto-Huikko M, Nilsson S, Gustafsson J-A (1996) Cloning of a novel estrogen receptor expressed in rat prostate and ovary. *Proc Natl Acad Sci USA* 93:5925–5930.
8. Mosselman S, Polman J, Dijkema R (1996) ERβ: Identification and characterization of a novel human estrogen receptor. *FEBS Lett* 392:49–53.
9. Tremblay GB, *et al.* (1997) Cloning, chromosomal localization, and functional analysis of the murine estrogen receptor β. *Mol Endocrinol* 11:353–365.
10. Imamamov O, Shim G-J, Warner M, Gustafsson J-A (2005) Estrogen receptor beta in health and disease. *Biol Reprod* 73:866–871.
11. Koehler KF, Helguero LA, Haldosén L-A, Warner M, Gustafsson J-A (2005) Reflections on the discovery and significance of estrogen receptor beta. *Endocrine Rev* 26:465–478.
12. Harris HA (2007) Estrogen receptor-β: Recent lessons from *in vivo* studies. *Mol Endocrinol* 21:1–13.
13. Krege JH, *et al.* (1998) Generation and reproductive phenotypes of mice lacking estrogen receptor β. *Proc Natl Acad Sci USA* 95:15677–15682.
14. Dupont S, *et al.* (2000) Effect of single and compound knockouts of estrogen receptors α (ERα) and β (ERβ) on mouse reproductive phenotypes. *Development* 127:4277–4291.
15. Shughrue PJ, Askew GR, Dellovade TL, Merchenthaler I (2002) Estrogen-binding sites and their functional capacity in estrogen receptor double knockout mouse brain. *Endocrinology* 143:1643–1650.
16. Imamamov O, *et al.* (2004) Estrogen receptor β regulates epithelial cellular differentiation in the mouse ventral prostate. *Proc Natl Acad Sci USA* 101:9375–9380.
17. Wang L, Andersson S, Warner M, Gustafsson J-A (2001) Morphological abnormalities in the brains of estrogen receptor β knockout mice. *Proc Natl Acad Sci USA* 98:2792–2796.
18. Wang L, Andersson S, Warner M, Gustafsson J-A (2003) Estrogen receptor (ER) β knockout mice reveal a role for ERβ in migration of cortical neurons in the developing brain. *Proc Natl Acad Sci USA* 100:703–708.
19. Weihua Z, *et al.* (2001) A role for estrogen receptor β in the regulation of growth of the ventral prostate. *Proc Natl Acad Sci USA* 98:6330–6335.
20. Shim G-J, *et al.* (2003) Disruption of the estrogen receptor β gene in mice causes myeloproliferative disease resembling chronic myeloid leukemia with lymphoid blast crisis. *Proc Natl Acad Sci USA* 100:6694–6699.
21. Förster C, Kietz S, Hultenby K, Warner M, Gustafsson J-A (2004) Characterization of the ER$\beta^{-/-}$ mouse heart. *Proc Natl Acad Sci USA* 101:14234–14239.
22. Patrone C, *et al.* (2003) Regulation of postnatal lung development and homeostasis by estrogen receptor β. *Mol Cell Biol* 23:8542–8552.
23. Morani A, *et al.* (2006) Lung dysfunction causes systemic hypoxia in estrogen receptor β knockout (ER$\beta^{-/-}$) mice. *Proc Natl Acad Sci USA* 103:7165–7169.
24. Wada-Hiraike O, *et al.* (2006) Role of estrogen receptor β in colonic epithelium. *Proc Natl Acad Sci USA* 103:2959–2964.
25. Imamamov O, *et al.* (2007) Estrogen receptor β-deficient female mice develop a bladder phenotype resembling human interstitial cystitis. *Proc Natl Acad Sci USA* 104:9806–9809.
26. Inzunza J, *et al.* (2007) Ovarian wedge resection restores fertility in estrogen receptor β knockout (ER$\beta^{-/-}$) mice. *Proc Natl Acad Sci USA* 104:600–605.
27. Allen E (1922) The oestrus cycle in the mouse. *Am J Anat* 30:297–371.
28. Fata JE, Chaudhary V, Khorkha R (2001) Cellular turnover in the mammary gland is correlated with the systemic levels of progesterone and not 17β-estradiol during the estrous cycle. *Biol Reprod* 65:680–688.
29. Palmieri C, *et al.* (2002) Estrogen receptor beta in breast cancer. *Rev Endocrine Related Cancer* 9:1–13.
30. Förster C, *et al.* (2002) Involvement of estrogen receptor β in terminal differentiation of mammary gland epithelium. *Proc Natl Acad Sci USA* 99:15578–15583.
31. Radovsky A, Mitsumori K, Chapin RC (1999) in *Pathology of the Mouse*, eds Maronpot RR, Boorman GA, Gaul B (Cache River, Vienna), p 389.
32. Rehm S, *et al.* (2001) in *International Classification of Rodent Tumours. The Mouse*, eds Mohr U (Springer, Heidelberg), pp 184–185.
33. Weihua Z, Warner M, Gustafsson J-A (2002) Estrogen receptor beta in the prostate. *Mol Cell Endocrinol* 193:1–5.
34. Stanbrough M, Leav I, Kwan PWL, Bubley GJ, Balk SP (2001) Prostatic intraepithelial neoplasia in mice expressing an androgen receptor transgène in prostate epithelium. *Proc Natl Acad Sci USA* 98:10823–10828.
35. Radovsky A, Mahler JF (1999) in *Pathology of the Mouse*, eds Maronpot RR, Boorman GA, Gaul B (Cache River, Vienna), p 450.
36. Carson FL (1996) in *Histotechnology a Self-Instructional Text* (Am Soc Clin Pathol, Chicago), p 120.
37. Saunders PTK (2005) Does estrogen receptor β play a significant role in human reproduction? *Trends Endocrinol Metab* 16:222–227.
38. Hull EM, Dominguez JM (2007) Sexual behaviour in male rodents. *Horm Behav* 52:45–55.
39. Temple JL, Scordalakes EM, Bodo C, Gustafsson J-A, Rissman EF (2003) Lack of functional estrogen receptor β gene disrupts pubertal male sexual behaviour. *Horm Behav* 44:427–434.
40. Nomura M, *et al.* (2006) Estrogen receptor-β gene disruption potentiates estrogen-inducible aggression but not sexual behaviour in male mice. *Eur J Neurosci* 23:1860–1868.
41. Ogawa S, *et al.* (1999) Survival of reproductive behaviors in estrogen receptor β gene-deficient (βERKO) male and female mice. *Proc Natl Acad Sci USA* 96:12887–12892.
42. Kudwa AE, Bodo C, Gustafsson J-A, Rissman EF (2005) A previously uncharacterized role for estrogen receptor β: Defeminization of male brain and behaviour. *Proc Natl Acad Sci USA* 102:4608–4612.
43. Couse JF, Hewitt SC, Korach KS (2000) Receptor null mice reveal contrasting roles for estrogen receptor α and β in reproductive tissues. *J Steroid Biochem Mol Biol* 74:287–296.